THE JOURNAL OF BIOLOGICAL CHEMISTRY Vol. 280, No. 24, Issue of June 17, pp. 22769–22775, 2005
Printed in U.S.A.

Disease-associated Mutations and Alternative Splicing Alter the Enzymatic and Motile Activity of Nonmuscle Myosins II-B and II-C*

Received for publication, March 30, 2005
Published, JBC Papers in Press, April 20, 2005, DOI 10.1074/jbc.M503488200

Kye-Young Kim‡§¶, Mihály Kovács§‖, Sachiyo Kawamoto‡, James R. Sellers‖, and Robert S. Adelstein‡

From the ‡Laboratory of Molecular Cardiology and ‖Laboratory of Molecular Physiology, NHLBI, National Institutes of Health, Bethesda, Maryland 20892

Human families with single amino acid mutations in nonmuscle myosin heavy chain (NMHC) II-A (*MYH9*) and II-C (*MYH14*) have been described as have mice generated with a point mutation in NMHC II-B (*MYH10*). These mutations (R702C and N93K in human NMHC II-A, R709C in murine NMHC II-B, and R726S in human NMHC II-C) result in phenotypes affecting kidneys, platelets, and leukocytes (II-A), heart and brain (II-B), and the inner ear (II-C). To better understand the mechanisms underlying these defects, we characterized the *in vitro* activity of mutated and wild-type baculovirus-expressed heavy meromyosin (HMM) II-B and II-C. We also expressed two alternatively spliced isoforms of NMHC II-C which differ by inclusion/exclusion of eight amino acids in loop 1, with and without mutations. Comparison of the actin-activated MgATPase activity and *in vitro* motility shows that mutation of residues Asn-97 and Arg-709 in HMM II-B and the homologous residue Arg-722 (Arg-730 in the alternatively spliced isoform) in HMM II-C decreases both parameters but affects *in vitro* motility more severely. Analysis of the transient kinetics of the HMM II-B R709C mutant shows an extremely tight affinity of HMM for ADP and a very slow release of ADP from acto-HMM. Although mutations generally decreased HMM activity, the R730S mutation in HMM II-C, unlike the R730C mutation, had no effect on actin-activated MgATPase activity but decreased the rate of *in vitro* motility by 75% compared with wild type. Insertion of eight amino acids into the HMM II-C heavy chain increases both actin-activated MgATPase activity and *in vitro* motility.

Class II myosins are hexameric proteins composed of two heavy chains and two pairs of light chains that hydrolyze MgATP and interact with actin to produce movement. Mammalian nonmuscle myosins II play an important role in diverse types of movement, including cytokinesis, cell migration, and cell shape change (1–3). They consist of three widely expressed heavy chain isoforms, nonmuscle myosin heavy chains (NMHC)[1] II-A, II-B, and II-C, which are the products of three different genes termed *MYH9* (4, 5), *MYH10* (5), and *MYH14* (6, 7) in humans, respectively. The three NMHC isoforms are 64–80% identical at the level of amino acids but are sufficiently different in sequence at the N-terminal and C-terminal ends to permit generation of specific antibodies (7). Information on the biological role of nonmuscle myosin II-C is presently limited due to its more recent identification. Nevertheless, the protein expression pattern in human and mouse tissues for NMHC II-C shows that this protein is absent during the earliest stages of development (7, 8).

NMHC II-C has two alternatively spliced isoforms, with the inserted isoform (NMHC II-C1) differing from the noninserted isoform (NMHC II-C0) by 8 amino acids (ASVSTMSY in mice) that are inserted into loop 1 in the globular head (7). The insert starts just after amino acid 227 at a position homologous to the inserted amino acids in vertebrate NMHC II-B and the smooth muscle myosin heavy chain (9, 10). The inserted NMHC II-C mRNA is highly expressed in adult murine liver, kidney, testes, brain, and lung, but heart and skeletal muscle contains only small amounts of the inserted message (7). To date there has been no biochemical characterization of the differences between the inserted and noninserted NMHC II-C isoforms.

Single amino acid mutations have been reported in humans for NMHC II-A and II-C. The mutations in NMHC II-A are spread throughout the NMHC and result in defects in a variety of cells and organs including platelets, kidney, lens, and the inner ear (11). The *in vitro* effects of a number of these mutations on the myosin enzymatic activity and assembly have been reported (12, 13). Of particular interest are the mutations N93K and R702C in NMHC II-A, which have been expressed as heavy meromyosin fragments (HMM) using baculovirus and characterized with respect to their actin-activated MgATPase activity and their ability to translocate actin filaments (13). Moreover, the R726S mutation in NMHC II-C at an amino acid homologous to the R702C mutation in NMHC II-A results in an autosomal dominant hearing loss in humans (14). Our laboratory has generated mice with a mutation in NMHC II-B (R709C), which is homologous to the residue mutated in NMHC II-A (R702C). The NMHC II-B mutant mice develop major defects in the brain and heart during embryonic development (15, 16).

The purpose of the present study is to quantitate the kinetic parameters of the various mutated and alternatively spliced isoforms of nonmuscle myosin II-B and II-C and to

* The costs of publication of this article were defrayed in part by the payment of page charges. This article must therefore be hereby marked "*advertisement*" in accordance with 18 U.S.C. Section 1734 solely to indicate this fact.

This article is dedicated to the memory of Yvette A. Preston.

§ These authors made major contributions to this work.

¶ Partially supported by the Korea Research Foundation Grant funded by Korea Government (Ministry of Education and Human Resources Development, Basic Research Promotion Fund M01–2003-000-10307-0).

** To whom correspondence should be addressed: National Institutes of Health, Bldg. 10, Rm. 8N202, 10 Center Dr. MSC 1762, Bethesda, MD. 20892-1762; Tel.: 301-496-1865; Fax: 301-402-1542; E-mail: AdelsteR@NHLBI.NIH.gov.

[1] The abbreviations used are: NMHC, nonmuscle myosin heavy chain; HMM, heavy meromyosin; MLC, myosin light chain; MLCK, MLC kinase; IVM, *in vitro* motility; MOPS, 4-morpholinepropanesulfonic acid; WT, wild type; NSM, no significant movement.

compare the effects of these mutations among all three nonmuscle myosins. To accomplish this we expressed the relevant HMMs along with the 20- and 17-kDa myosin light chains using the baculovirus expression system. The kinetic properties of two different mutations in HMM II-B, N97K and R709C, were compared with wild-type HMM II-B as well as to the previously reported results for homologous mutations in HMM II-A (13). We also introduced mutations into NMHC II-C, but here we also address the effects of alternative splicing. First, we compared the actin-activated MgATPase activity and *in vitro* motility of the inserted and noninserted isoforms of murine HMM II-C. We then introduced the mutation R722C, which is homologous to R709C in NMHC II-B and R702C in NMHC II-A, into both the inserted (R730C) and noninserted (R722C) NMHC II-C isoforms. After we initiated this work, a report appeared describing humans with an autosomal dominant hearing loss who had a mutation in NMHC II-C at R726S (14). This is homologous to Arg-722 (or Arg-730 in the inserted isoform) in mice, so we also expressed murine-inserted HMM II-C that had the R730S mutation.

EXPERIMENTAL PROCEDURES

Construction of Baculovirus Expression Vectors—A recombinant HMM-like protein of human NMHC II-B and mouse NMHC II-C was expressed in the baculovirus/Sf9 system. Briefly, the cDNA (nucleotides 1–3135) for human NMHC II-B (GenBank™ accession number M69181, with a change in Cys-800 to Tyr, which is the more common amino acid used) and the cDNA (nucleotides 1–4071) for mouse NMHC II-C (GenBank™ accession number AY205605) were truncated at codon 1045 and at codon 1357, respectively, to create an HMM fragment. Nucleotides encoding a FLAG epitope (DYKDDDDK) followed by a stop signal were appended to aid in purification. The HMM constructs were subcloned into the baculovirus transfer vector pFastBac1 (Invitrogen).

Site-directed Mutagenesis—We used a PCR-based mutagenesis technique to generate the mutant constructs of HMM II-B and II-C. For the N97K mutant HMM II-B, the nucleotides coding for Asn at codon 97 were mutated to nucleotides coding for Lys. The primers used were 5′-GCAGAATTGACATGCTTG**AAG**GAGGCTTCCGTTTTACATAATC-TG-3′ and the complementary antisense primer. Similarly, for the R709C mutant HMM II-B, Arg-709 was mutated to Cys using the primer 5′-GTCCTGGAAGGGATC**TGT**ATCTGTCGCCAGGGCTTCCC-T-3′ and the complementary antisense primer. The mutated nucleotides responsible for conversion to different amino acids are shown in bold and underlined. The complete nucleotide sequence of the mutant cDNAs was confirmed by DNA sequencing. To generate a clone of the 8-amino acid inserted isoform in NMHC II-C, we introduced the 24-nucleotide cassette encoding the insert into the TOPO TA vector (Invitrogen) with the noninserted fragment (nucleotide 1–1227) by the QuikChange system (Stratagene). The clone with the insert together with the 3′ portion of HMM II-C was then subcloned into pFastBac1. Arg-722 in HMM II-C (or Arg-730 in the inserted HMM II-C) was mutated to Cys or Ser using the primer 5′-GGGGTCCTCGAAGGTAT-A**TGC**ATCTGTCGCCAAGGCTTC-3′ or 5′-GGGGTCCTCGAAGGTAT-A**AGC**ATCTGTCGCCAAGGCTTC-3′, respectively.

Preparation and Purification of HMM Proteins—The wild-type and mutant recombinant HMMs of NMHC II-B and the two isoforms of NMHC II-C were expressed in the baculovirus/Sf9 system including the appropriate light chains (17) and purified according to Wang *et al.* (18). Each virus was cotransfected along with a virus containing both light chains into 3×10^9 Sf9 cells. The infected cells were harvested by sedimentation after 72 h of growth and stored at −80 °C. Western blot analyses of the Sf9 cell pellets before extraction of the proteins demonstrated that significant amounts of the protein were expressed. The partially thawed pellet was extracted with 0.5 M NaCl, 10 mM MOPS (pH 7.3) 10 mM $MgCl_2$, 1 mM EGTA, 3 mM NaN_3, 2 mM ATP, 0.1 mM phenylmethylsulfonyl fluoride, 0.1 mM dithiothreitol, 5 μg/ml leupeptin, and proteinase inhibitor mixture after homogenization in a ground glass homogenizer and purified by FLAG affinity chromatography. The material eluted from the FLAG column (Sigma) was concentrated using a Sepharose Q column (Amersham Biosciences). The protein concentration was determined by Bradford assay using smooth muscle HMM as a standard.

ATPase Assay—Actin-activated MgATPase activities were measured by an NADH-linked assay as described by Wang *et al.* (19) in a buffer containing 10 mM MOPS (pH 7.0), 2 mM $MgCl_2$, 0.1 mM EGTA, 1 mM ATP, 0.2 mM $CaCl_2$, 1 μM calmodulin, 10 μg/ml MLCK, 40 units/ml lactate dehydrogenase, 200 units/ml pyruvate kinase, 1 mM phosphoenolpyruvate, and 0.2 mM NADH plus various concentrations of actin. Actin filaments were stabilized by a 1.5-fold molar excess of phalloidin (Calbiochem). The actin concentration varied from 1 to 50 μM. The assays were performed at 25 °C for HMM II-B and 25 and 37 °C for HMM II-C. Data were corrected for the background ATPase activity of actin. Fitting of experimental data sets to mathematical functions was done using OriginLab 7.0 (Microcal Corp.). Reported means and S.D. are those of three to four separate experiments. For ATPase activities measured at 37 °C in the case of HMM II-C0 and II-C1,only two experiments from two different preparations are reported.

In Vitro Motility (IVM) Assay—Assays were performed at 30 °C in a buffer comprising 50 mM KCl, 20 mM MOPS (pH 7.4), 5 mM $MgCl_2$, 0.1 mM EGTA, 1 mM ATP, 50 mM dithiothreitol 0.2 μM chicken gizzard tropomyosin, 0.7% methylcellulose, 2.5 mg/ml glucose, 0.1 mg/ml glucose oxidase, and 2 μg/ml catalase. All HMM proteins were introduced at a protein concentration of 0.2 mg/ml into a flow chamber with a nitrocellulose-coated coverslip. The surface was subsequently blocked by 1 mg/ml bovine serum albumin and then incubated for 1 min at room temperature in a solution containing 5 μM unlabeled F-actin, 1 mM ATP, 0.2 mM $CaCl_2$, 1 μM calmodulin, and 4 μg/ml MLCK. After washout, 20 nM F-actin labeled with rhodamine-phalloidin (Molecular Probes) and the above assay buffer was applied to the flow chamber. The sliding speed of actin filaments over the myosin-coated surface was analyzed using the CellTrak system (Motion Analysis) as described earlier (17). Reported means and S.D. are those of three to four separate experiments.

Transient Kinetics—Stopped-flow experiments were performed in a SF-2001 apparatus (Kin-Tek Corp.) at 25 °C in buffer containing 20 mM MOPS (pH 7.0), 5 mM $MgCl_2$, 100 mM KCl, and 0.1 mM EGTA. Pyrene fluorescence was excited at 365 nm (6-nm bandwidth), and emission was monitored through a 400-nm long-pass filter. 2′(3)-*O*-(*N*-Methylanthraniloyl)-ADP (Molecular Probes) was excited via energy transfer from vicinal tryptophan residues (excitation at 280 nm with a 6-nm bandwidth), and the emitted light was selected using a 400-nm long-pass cutoff filter. Pre-mixing concentrations are indicated throughout this study unless stated otherwise. The volume ratio was 1:1 in all experiments. Actin was pyrene-labeled as in Cooper *et al.* (20). Actin filaments were stabilized by a 1.5-fold molar excess of phalloidin. HMM constructs were thiophosphorylated and re-purified as in Facemyer and Cremo (21). Fitting of experimental datasets to mathematical functions was done using the SF-2001 software and OriginLab 7.0. Reported means and S.D. are those for two to three different experiments.

RESULTS

Table I summarizes the mutations introduced into NMHC II-B and NMHC II-C. The table also includes a list of the developmental defects associated with these mutations, both in humans and mice. Note that because the identity of amino acids between the same NMHC isoforms from mice and humans exceeds 90%, we considered the species together for comparative purposes. Fig. 1 is a Coomassie Blue-stained gel showing each of the purified HMM constructs expressed using the baculovirus system. These include the wild-type and mutant HMM II-B as well as the wild-type and mutant HMM II-C with the inserted amino acids (C1) or without (C0). Each of these proteins could be purified in mg quantities, and each HMM heavy chain bound the co-expressed MLC_{20} and MLC_{17} in an approximate 1:1:1 ratio.

Enzymatic Activity of Wild-type and Mutant HMM II-B—The enzymatic activity was initially assessed by measuring the MgATPase activities of the proteins in the absence of actin before as well as after phosphorylation of the regulatory myosin light chain, catalyzed by MLCK. The basal activity was very low (<0.004 s^{-1}) for each of the HMM II-B and HMM II-C proteins. All the HMMs (both II-B and II-C as well as II-A (13)) required phosphorylation of the 20-kDa MLC for full activation of their actin-activated MgATPase activity (data not shown). Fig. 2*A* shows that both the N97K and R709C mutations decrease the actin-activated MgATPase activity of phosphoryl-

TABLE I

Mutations in the NMHC and their association with developmental defects

The asterisk (*) indicates HMM constructs used in the current study. Asn-97 of human NMHC II-B is homologous to Asn-93 of human NMHC II-A. Arg-709 of human NMHC II-B is homologous to Arg-722 of mouse NMHC II-C0, Arg-730 of mouse NMHC II-C1, Arg-726 of human NMHC II-C, and Arg-702 of human NMHC II-A. II-C0, noninserted NMHC II-C; II-C1, inserted NMHC II-C with an eight-amino acid insert.

NMHC	Species	Mutations	Associated defects
*II-B	Human	N97K	
*II-B	Human	R709C	
II-B	Mouse	R709C	Defect in brain and heart (15, 16)
*II-C0	Mouse	R722C	
*II-C1	Mouse	R730C	
*II-C1	Mouse	R730S	
II-C	Human	R726S	Autosomal dominant hearing impairment (14)
II-A	Human	N93K	Defect in platelets (11)
II-A	Human	R702C	Defect in kidney, platelets, hearing, and sight (11)

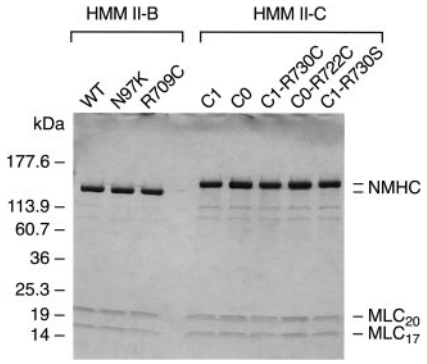

FIG. 1. **Expression and purification of FLAG-tagged HMM II-B and HMM II-C from baculovirus-infected Sf9 cells.** HMM II-B and HMM II-C wild type and mutant proteins were purified by FLAG affinity chromatography followed by concentration on a Sepharose Q column. A 4–20% polyacrylamide gradient-SDS gel was used to separate the purified HMM II-B and II-C heavy chains and two light chains and was stained with Coomassie Blue. The position of the HMM heavy chain (NMHC) and the regulatory (MLC_{20}) and essential light chain (MLC_{17}) are marked. Minor bands of intermediate molecular weight indicate a very small amount of proteolytic breakdown. *C0*, noninserted NMHC II-C; *C1*, inserted NMHC II-C with an eight-amino acid insert.

ated HMM II-B, with the latter mutation having a greater effect. The data for each HMM were fitted to a hyperbolic equation to determine the kinetic constants: V_{max} (maximal actin-activated ATPase activity) and K_{ATPase} (actin concentration at half-maximal activation; see Table II). Fig. 2*B* shows an expanded data set at lower actin concentrations, confirming the values in Fig. 2*A*. The V_{max} of R709C-HMM was about 29% that of WT-HMM (0.05 ± 0.003 s^{-1} for R709C compared with 0.17 ± 0.04 s^{-1} for the wild-type), and its K_{ATPase} was much lower than that of WT-HMM (<0.5 μM for R709C compared with 3.4 ± 1.8 μM for the wild-type), indicating that it has a considerably higher actin affinity in the presence of ATP (see Table II). In contrast, the V_{max} (0.12 ± 0.04 s^{-1}) and K_{ATPase} (1.8 ± 0.6 μM) values of N97K-HMM were about 70 and 55% of that of WT-HMM, respectively.

An important functional property of myosin is its ability to translocate actin filaments. This can be measured using the *in vitro* motility assay with rhodamine-phalloidin-labeled actin. The movement of actin filaments over the myosin-coated surface was detected by fluorescence microscopy and the sliding speed was analyzed using the CellTrak system. All myosins were phosphorylated using MLCK prior to assay. As Table II shows, WT-HMM II-B moved actin filaments with an average velocity of 0.17 μm/s. The average sliding velocity of actin filaments propelled by mutant N97K-HMM was 0.06 μm/s (Fig. 2*C*). In contrast, we did not observe any significant movement (<0.01 μm/s) of actin filaments bound to R709C-HMM coated

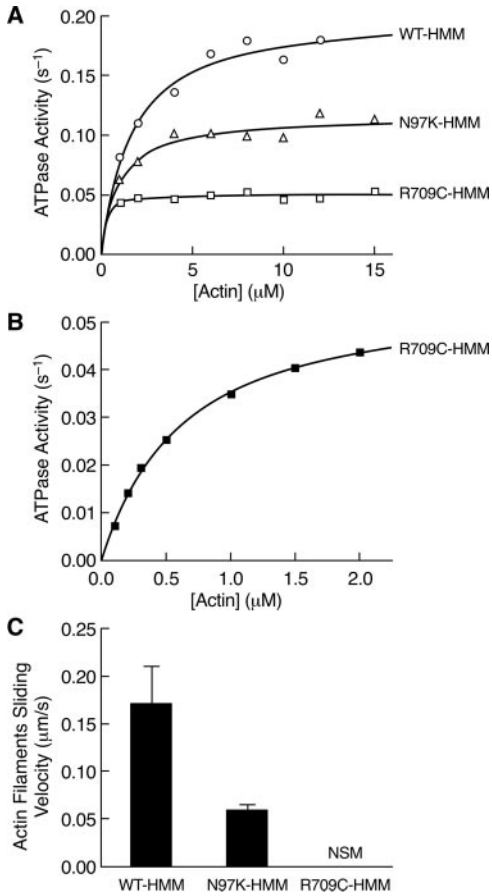

FIG. 2. **Enzymatic and motile activity of wild-type and mutant HMM II-B molecules.** *A*, actin-activated MgATPase activity of WT-HMM (*circles*), N97K-HMM (*triangles*), and R709C-HMM (*squares*) was measured at 25 °C. The actin concentration was varied from 1 to 15 μM. *B*, actin-activated MgATPase activity of R709C-HMM at low actin concentrations. The activity was measured at actin concentrations from 0.1 to 2 μM. The MgATPase activity of myosin in the absence of actin was subtracted from each data point. Data sets were fitted to a hyperbolic equation (*solid lines*) to determine the kinetic constants, V_{max} and K_{ATPase} (see Table II). The data shown are from a single preparation of each HMM. *C*, *in vitro* motility of wild-type and mutant HMM II-B molecules. Each HMM II-B protein was applied at a concentration of 0.2 mg/ml into the flow chamber. The sliding velocity was determined for three to four preparations each of WT-HMM, N97K-HMM, and R709C-HMM. The plot shows the mean velocity with the S.D. NSM of actin filaments was seen with the R709C-HMM preparation. All proteins were phosphorylated with MLCK prior to the assays.

surfaces (Fig. 2*C*). Neither could we detect any motility of R709C-HMM in a similar motility assay using a laser scanning confocal microscope set up over a time course of 60 min. These

TABLE II

Summary of actin-activated MgATPase activity and in vitro motility of HMMs

The values for V_{max}, K_{ATPase}, and IVM *(in vitro* motility) are the mean and S.D. from two to four protein preparations. The numbers in parentheses refer to references. C0, noninserted NMHC II-C; C1, inserted NMHC II-C with an eight-amino acid insert.

HMMs	°C[a]	V_{max}	K_{ATPase}	IVM (30 °C)
		s^{-1}	μM	$\mu m/s$
HMM II-B	25			
WT-HMM		0.17 ± 0.04	3.4 ± 1.8	0.17 ± 0.03
N97K-HMM		0.12 ± 0.04	1.8 ± 0.6	0.06 ± 0.004
R709C-HMM		0.05 ± 0.003	<0.5	NSM
HMM II-C	37			
C1-HMM		0.85 ± 0.18	26.1 ± 6.2	0.08 ± 0.003
C0-HMM		0.29 ± 0.04	9.9 ± 6.0	0.03 ± 0.005
HMM II-C	25			
C1-HMM		0.26 ± 0.002	5.7 ± 2.9	0.08 ± 0.01
C0-HMM		0.18 ± 0.04	4.2 ± 1.1	0.03 ± 0.006
C1-R730C-HMM		0.08 ± 0.007	1.6 ± 0.2	NSM
C0-R722C-HMM		0.03 ± 0.001	0.4 ± 0.02	NSM
C1-R730S-HMM		0.28 ± 0.04	3.5 ± 1.2	0.02 ± 0.003
HMM II-A (37)	25			
WT-HMM		0.45 ± 0.03	9 ± 2	
HMM II-A (13)	35			
WT-HMM		0.92 ± 0.15	8.4 ± 0.5	0.34 ± 0.09
N93K-HMM		0.03 ± 0.002	1.7 ± 0.2	NSM
R702C-HMM		0.20 ± 0.05	3.0 ± 0.1	0.17 ± 0.03

[a] Measured temperature for MgATPase activity assay.

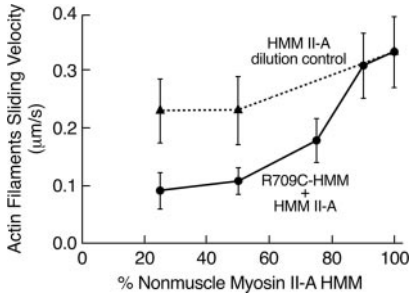

FIG. 3. **Movement of actin filaments in mixtures of HMM II-A and R709C mutant HMM II-B.** Nonmuscle myosin II-A (HMM II-A) was mixed with R709C-HMM (*circles*) at various ratios, keeping the total HMM concentration at 0.2 mg/ml before binding to the coverslip of the flow chamber. *Triangles* represent dilution control experiments in which HMM II-A at different concentrations (0.05, 0.1, and 0.2 mg/ml from *left* to *right*) was not supplemented with R709C-HMM. Each data point represents the mean velocity and S.D. at that mixing ratio. *Error bars* show S.D. for 20–50 actin filaments. The experiment was repeated twice.

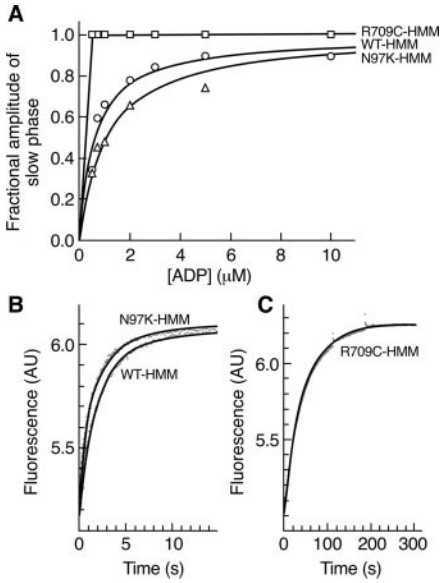

FIG. 4. **ADP interaction of wild-type and mutant HMM II-B molecules.** *A*, ADP binding affinity to acto-HMM II-B. 0.2 μM pyrene-acto-HMM was preincubated with the indicated ADP concentrations and then rapidly mixed with a large excess of ATP (500 μM) in the stopped-flow apparatus. Hyperbolic fits to the fractional amplitude of the slow phase (expressed as $A_{slow}/(A_{fast} + A_{slow})$) *versus* ADP concentration indicated a K_d for ADP binding to pyrene-acto-HMM as follows: 0.61 ± 0.13 μM for WT-HMM (*circles*) and 1.1 ± 0.1 μM for N97K-HMM (*triangles*). Practically all the acto-R709C-HMM was ADP-bound even at 0.5 μM ADP concentration (*squares*), which indicates a $K_d < 0.1$ μM in this construct. *B* and *C*, ADP dissociation from acto-HMM II-B. Pyrene-actin fluorescence transients recorded on mixing 0.2 μM pyrene-acto-HMM plus 20 μM ADP with 500 μM ATP at 25 °C are shown. Under these conditions, the reaction was rate-limited by ADP dissociation from acto-HMM, which had a rate constant (k_{off}) of 0.52 ± 0.05 s^{-1} for wild-type HMM II-B, 1.9 ± 0.3 s^{-1} for the N97K mutant HMM, and 0.02 ± 0.005 s^{-1} for the mutant R709C-HMM (see Table III). All HMMs were thiophosphorylated before the assay. Note the different time scales of *panels B* and *C*. *AU*, arbitrary units.

results indicate that the R709C mutation in HMM II-B causes a large reduction in the actin-activated MgATPase activity and a loss of unloaded *in vitro* motor activity.

Inhibition of HMM II-A Movement by R709C-HMM—To better understand the mechanism underlying the absence of detectable movement of actin filaments by R709C-HMM in the IVM assay, we mixed the R709C mutant HMM II-B at varying ratios with wild-type HMM II-A, the nonmuscle HMM found to propel actin filaments with the highest velocity among nonmuscle HMMs (13). As shown in Fig. 3, the presence of the mutant R709C-HMM, even in low amounts, markedly slowed the movement of HMM II-A, showing that the R709C-HMM is predominantly in a strongly actin-bound state during steady-state ATP hydrolysis, which is also indicated by the very low K_{ATPase} value (<0.5 μM) shown in Table II.

ADP Kinetics of Wild-type and Mutant HMM II-B—To gain further insight into the kinetic differences among the R709C mutant, the N97K mutant and wild-type HMM II-B, we determined the ADP binding affinity of actin-bound wild-type and mutant HMM II-B proteins (acto-HMM). We used a stopped-flow-based ADP titration method obtaining the results shown in Fig. 4*A*. The ATP-induced dissociation of the HMM heads of all three constructs from pyrene-actin caused a multiexponential increase in pyrene-actin fluorescence. The fast phase of the transients (with observed rate constants of 50–100 s^{-1}) represents the ATP-induced dissociation of the ADP-free fraction of myosin heads from actin, whereas the slow phase (rate constants <3 s^{-1}) reflects the ADP-bound fraction in which ADP

TABLE III
ADP kinetics of wild-type and mutant HMM II-B constructs

Stopped-flow experiments were done at 25 °C using a SF-2001 apparatus. Reported means and S.D. are those for two to three different experiments. S1, subfragment 1 (the number in parentheses refers to Ref. 19).

	WT-S1 (19)	WT-HMM	N97K-HMM	R709C-HMM
−Actin				
k_{on} ($\mu M^{-1}s^{-1}$)[a]	0.81 ± 0.23			0.40 ± 0.1
k_{off} (s^{-1})[a]	0.48 ± 0.11			0.02 ± 0.003
K_d (μM)[b]	0.59			0.05
+Actin				
k_{on} ($\mu M^{-1}s^{-1}$)	2.4 ± 0.1[a]	0.85[b]	1.7[b]	1.8 ± 0.1[a]
k_{off} (s^{-1})	0.38 ± 0.09[a]	0.52 ± 0.05[c]	1.9 ± 0.3[c]	0.02 ± 0.005[a,c]
K_d (μM)	0.16[b]	0.61 ± 0.13[c]	1.1 ± 0.1[c]	0.012[b]
Thermodynamic coupling between actin and ADP binding[d]	0.27			0.25
Rate enhancement of ADP release by actin[e]	0.79			1.1

[a] Measured using 2′(3)-*O*-(*N*-methylanthraniloyl)-ADP as described in Wang *et al*. (19).
[b] Calculated from other parameters.
[c] Measured using pyrene-actin.
[d] Expressed as $K_{d(+actin)}/K_{d(-actin)}$.
[e] Expressed as $k_{off(+actin)}/k_{off(-actin)}$.

dissociation from the myosin head rate-limits the subsequent ATP binding and actomyosin dissociation process. Analysis of the amplitude data showed that the K_d of ADP binding to acto-N97K-HMM was modestly higher than that to acto-WT-HMM (1.1 ± 0.1 μM compared with 0.61 ± 0.13 μM, respectively), whereas the acto-R709C-HMM appeared to have a very high ADP affinity (K_d<0.1 μM, Fig. 4*A*). Accordingly, the off-rate constant (k_{off}) of ADP dissociation from acto-N97K-HMM was slightly elevated compared with the wild-type (1.9 ± 0.3 s^{-1} compared with 0.52 ± 0.05 s^{-1}, respectively), whereas acto-R709C-HMM exhibits an extremely slow release of ADP (k_{off} = 0.02 ± 0.005 s^{-1}) from acto-HMM (Fig. 4, *B* and *C*, Table III). To assess the effect of actin on the ADP kinetics of R709C-HMM, we have also determined its ADP binding properties using 2′(3)-*O*-(*N*-methylanthraniloyl)-ADP, a fluorescent ADP analog both in the presence and absence of actin. We did not observe a significant change in the thermodynamic coupling ratio between actin and ADP binding and the enhancement of the ADP release rate by actin in R709C-HMM compared with that in wild-type subfragment 1 of NMHC II-B (Table III).

Interestingly, the ADP release rate constant in R709C-HMM (k_{off} = 0.02 ± 0.005 s^{-1}) was even slower than the maximal steady-state actin-activated ATPase activity (V_{max} = 0.05 ± 0.003 s^{-1}). A possible explanation for this finding is that the release of ADP from one or both heads of R709C-HMM is slightly slowed when starting from an acto-HMM·ADP complex in which both heads are initially actin-bound, whereas this molecular arrangement is unlikely to occur during the steady-state ATPase assay. Further support for this possibility is the fact that the ADP release transients show signs of biphasicity (Fig. 4, *B* and *C*), which may reflect differences in the ADP dissociation kinetics of the two heads of HMM.

Insertion of an Alternatively Spliced Exon and Mutations Alters HMM II-C Activity—Because the isoform of NMHC II-C with eight amino acids inserted into loop 1 is prominently expressed in a number of tissues, we first compared the kinetic properties of the inserted (C1) and noninserted (C0) wild-type HMMs and then compared these to the mutated constructs (see below). Table II shows that at both 37 °C (Fig. 5*A*) and 25 °C (Fig. 5*B*), insertion of 8 amino acids in loop 1 results in a higher V_{max} and IVM activity for HMM II-C. Introducing the R722C (R730C in C1-HMM) mutation decreases the actin-activated MgATPase activity of both C0 (noninserted) and C1 (inserted) HMMs (Table II, Fig. 5*B*). In contrast, introduction of the R730S mutation has no significant effect on V_{max} compared with wild-type C1-HMM. Thus, altering the Arg-730 mutation from Cys to Ser increased the V_{max} from 0.08 ± 0.007 to 0.28 ± 0.04 s^{-1} (compared with 0.26 ± 0.002 s^{-1} for the wild-type C1-HMM).

Fig. 5*C* and Table II shows the sliding velocities of actin filaments detected in the *in vitro* motility assay for the inserted (C1) and noninserted (C0) isoforms of HMM II-C as well as for the Arg-722 and Arg-730 mutants. The data indicate that introduction of 8 amino acids into loop 1 significantly increases the IVM rate from 0.03 to 0.08 μm/s. On the other hand, all three mutant HMMs studied showed a decrease in IVM rate, although the decrease in actin filament sliding velocity seen with the R730S mutant HMM was less marked (0.08 μm/s in wild-type C1-HMM compared with 0.02 μm/s in C1-R730S) than that for the other two mutant HMMs, C0-R722C and C1-R730C, which show a lack of detectable motility (<0.01 μm/s, Table II, Fig. 5*C*). Thus, this mutation (R730S) preserves the actin-activated MgATPase activity but decreases the IVM velocity by 4-fold. As noted in Table I, this is the same mutation that has been found in humans with impaired hearing (14).

DISCUSSION

The kinetic properties of NMHC II-A, II-B, and II-C are significantly different and suggest that these nonmuscle myosins could have distinct functions (19, 22, 23). Most cells in the tissues of humans and mice contain more than a single isoform, and although some overlap can be seen, most nonmuscle myosins II occupy specific locations in a given cell. Thus, their localization and extent of expression coupled with their distinct kinetic properties could explain their different functions. This is consistent with the findings from a number of laboratories that demonstrated different cellular localizations for myosin II-A and II-B (24–26) and more recent studies that showed distinct functions and localizations for myosin II-A and II-B in mouse fibroblasts (27, 28) as well as a number of other cells (26, 29).

In vivo experiments are also consistent with each isoform having a different function based on either localization, extent of expression, or both. Ablation of nonmuscle myosin II-A or II-B in mice results in different phenotypes during embryonic development. Whereas deletion of myosin II-A leads to defects in the visceral endoderm and cell-cell adhesion in the embryo, resulting in lethality as early as E6.5 (8), loss of myosin II-B allows development to progress to E14.5, with death being accompanied by abnormalities in the heart and brain (16, 30). More directly applicable to the present work are our findings with mice generated with a single amino acid mutation (R709C) in myosin II-B, which is homologous with the human R702C mutation in myosin II-A. A striking phenotype in these mice is a defect in the migration of three specific groups of

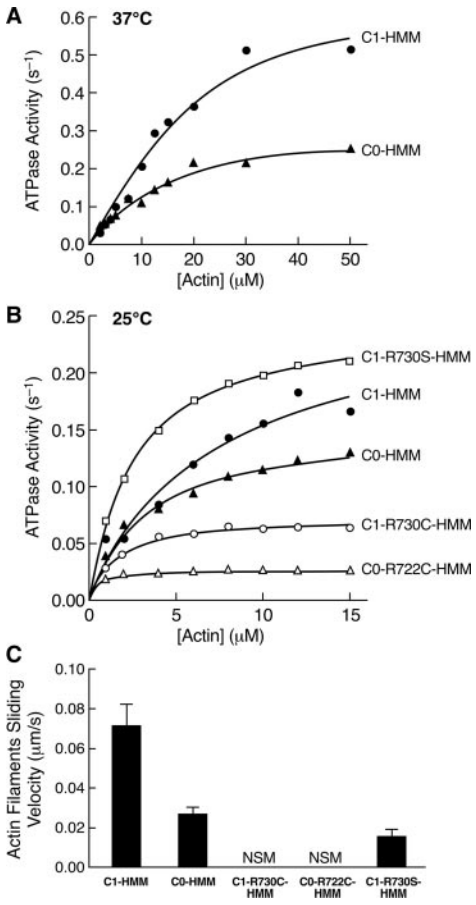

FIG. 5. **Enzymatic and motile activity of HMM II-C molecules.** *A*, the actin-activated MgATPase activity of C1-HMM (*closed circles*) and C0-HMM (*closed triangles*) was measured at 37 °C. The actin concentration was varied from 2 to 50 μM. *B*, actin-activated MgATPase activity of C1-HMM (*closed circles*), C0-HMM (*closed triangles*), C1-R730C-HMM (*open circles*), C0-R722C-HMM (*open triangles*), and C1-R730S-HMM (*open squares*) was measured at 25 °C. The actin concentration varied from 1 to 15 μM. The activity of myosin in the absence of actin was subtracted from each data point. Data sets were fitted to a hyperbolic equation to determine the kinetic constants, V_{max} and K_{ATPase} (see Table II). The data shown are from a single preparation of HMM II-C. *C*, average rates of actin filaments sliding over different HMM II-C constructs. The average rate of actin filament sliding was determined from two to three preparations of each HMM II-C construct. The plot shows the mean velocity with the S.D. All HMM II-C proteins were applied at a total protein concentration of 0.2 mg/ml into a flow chamber, respectively. NSM of actin filaments was seen with the C1-R730C-HMM and C0-R722C-HMM. All proteins were phosphorylated on the coverslip surface by incubation with MLCK. *C0*, noninserted NMHC II-C; *C1*, NMHC II-C with an 8-amino acid insert.

neuronal cells; that is, facial neurons, cerebellar granule cells, and pontine neurons. These cells appear to be more vulnerable to a mutation in myosin II-B because they have a higher content of this isoform compared with other brain neuronal cells (15). Moreover, the decrease in the rate of migration of these neuronal cells correlates with the decrease in enzymatic activity and *in vitro* motility found for the mutated HMM reported here. A second noteworthy point is the complete lack of overlap between the phenotype found in R702C myosin II-A mutated humans and R709C myosin II-B mutant mice, supporting the idea that myosin isoforms play distinct roles in specific cells, including cells that contain two or even three isoforms.

The expression of the HMM fragment was chosen because it is soluble at low ionic strength, which makes it more suitable for kinetic experiments. Moreover, it retains the regulatory behavior of the whole myosin molecule and is expressed at high levels in the baculovirus/Sf9 system. This high level of expression is in contrast to our original report in which we had problems expressing significant amounts of the noninserted HMM II-C0 (7). We solved this problem by re-engineering the construct in the pFastBac1 vector after removing an out of frame upstream ATG.

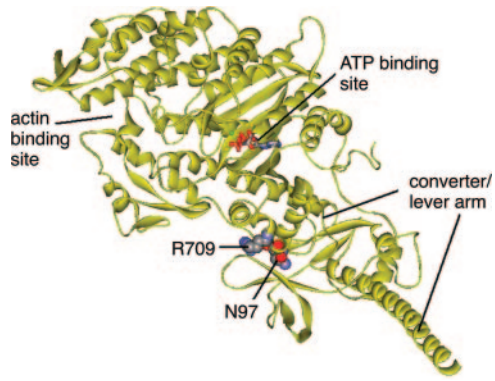

FIG. 6. **Localization of the mutant amino acids in the atomic structure of the myosin motor domain.** The crystal structure of a MgADP-bound myosin II motor domain from *Dictyostelium discoideum* was used to map the positions of the two mutations (PDB accession number 1G8X) (36). The myosin heavy chain segment is shown in *yellow*. Positions homologous to Asn-97 and Arg-709 of NMHC II-B are shown as space-filling models.

Both mutations (N97K and R709C) of HMM II-B impaired the activity of the myosin. When phosphorylated, R709C-HMM exhibited about 29% of maximal actin-activated MgATPase activity of WT-HMM, similar to the results with the R702C mutation in HMM II-A (Fig. 2*A*). The R709C-HMM also had a very low K_{ATPase} value (Fig. 2*B*) and provoked a marked inhibition of wild-type HMM II-A in the *in vitro* motility experiment (Fig. 3). We also observed that R709C-HMM exhibited a very high ADP affinity for actomyosin and an extremely slow ADP release (Fig. 4). These results demonstrate that a strong actin binding state (actomyosin·ADP) is the predominant ATPase intermediate in this mutant due to the blocking of ADP release from actomyosin.

A functionally important biochemical feature of NMHC II-B and NMHC II-A is that actin does not markedly accelerate the release of ADP from myosin (19, 22). Furthermore, contrary to all other myosins, there is a positive thermodynamic coupling between actin and ADP binding to NMHC II-B (*i.e.* binding of actin to myosin increases the ADP affinity and vice versa). Comparison of R709C-HMM with previously published data on wild-type myosin II-B subfragment 1 (19) reveals that these properties of NMHC II-B are hardly affected by the R709C mutation despite the pronounced effect of the mutation on ATPase activity, *in vitro* motility, and ADP release (Tables II and III).

NMHC II-C has two alternatively spliced forms and contains an insert of eight amino acids at the same location in loop 1 as described for smooth muscle myosin and NMHC II-B1 (9, 10). Kelley *et al.* (10) found that the smooth muscle HMM containing an insert of seven amino acids shows a higher velocity of movement of actin filaments *in vitro* and a higher actin-activated MgATPase activity than the noninserted smooth muscle myosin isoform. The presence of the insert correlates with a smooth muscle having phasic properties and its absence with a smooth muscle having tonic properties (10). On the other hand, NMHC II-B1 containing a 10-amino acid insert in loop 1 showed only a small increase in the actin-activated MgATPase activity and the *in vitro* motility (17). Interestingly, this insertion appears to play a specific role in proper migration of the facial neurons during mouse brain development.[2]

[2] X. Ma, unpublished results.

Based on its location in the crystal structure of myosin, Spudich (31) suggested that the sequence in loop 1, which is near the ATP binding pocket and, thus, may affect ADP release, might have a profound effect on the translocation of actin filaments by myosin in the *in vitro* motility assay. We found that inserted C1-HMM also has a higher actin-activated MgATPase activity and *in vitro* motility compared with the noninserted C0-HMM (Table II). R722C and R730C mutations of HMM II-C exhibited about 31 and 17% of the maximal actin-activated MgATPase activity of the two wild-type alternatively spliced isoforms of HMM II-C, respectively (Fig. 5*B*). We could not find any significant actin translocating activity using the two mutated HMM II-C constructs (Fig. 5*C*). The large effect of these mutations on *in vitro* motility is consistent with the results from the equivalent mutant of HMM II-B. Interestingly, the R730S mutant C1-HMM does retain actin-activated MgATPase activity similar to that of the wild-type C1-HMM, but its actin filament translocating velocity is only 25% that of wild-type C1-HMM (Table II).

In the atomic structure of the myosin motor domain, the residues homologous to Asn-97 and Arg-709 are located in close proximity to each other, near the base of the lever arm (Fig. 6). Asn-97is located in helix C of the N-terminal 25 kDa subdomain, whereas Arg-709 forms part of the so-called SH1-helix of the C-terminal converter region of the motor domain. These two side chains are part of the structural interface between the above two subdomains. This interface remains intact during the large conformational change of the motor domain, the so-called open-closed transition, the reversal of which may constitute the working stroke of myosin (32, 33). The maintenance of these subdomain contacts, similar to those between the converter and relay modules (34), are most likely essential for proper coordination of the events at the active site with lever arm movement. The subdomain contacts are maintained by a precise spatial arrangement of the side chains involved, which is evidenced by the very conservative sequence environment of both the Asn-97 and Arg-709 residues (1). Unwinding of the SH1 helix (the structural element in which Arg-709 resides) has been implicated in disruption of subdomain coordination and, in turn, uncoupling of the ATPase activity from motility (35). Consistent with this idea, the structurally disruptive mutations of Arg-709 in HMM II-B and Arg-722 or Arg-730 in HMM II-C cause an almost total loss of motile activity, whereas the mutant proteins still retain measurable actin-activated MgATPase activities (Table II). The information gathered from these experiments should not only help in the characterization of the biological properties of the mutant myosin but also help in our understanding of the phenotypes of the mice we are generating with point mutations, R709C in NMHC II-B and R722C in NMHC II-C.

Acknowledgments—We acknowledge the expert technical assistance of Estelle V. Harvey and Antoine Smith. Toshihiko Takenaka generated the original human II-B HMM construct. We also thank Catherine Magruder for expert editorial assistance and Mary Anne Conti and Earl Homsher for reading and improving this manuscript.

REFERENCES

1. Sellers, J. R. (1999) *Myosins*, 2nd Ed., Oxford University Press, Oxford
2. Berg, J. S., Powell, B. C., and Cheney, R. E. (2001) *Mol. Biol. Cell* **12,** 780–794
3. Bresnick, A. R. (1999) *Curr. Opin. Cell Biol.* **11,** 26–33
4. Toothaker, L. E., Gonzalez, D. A., Tung, N., Lemons, R. S., Le Beau, M. M., Arnaout, M. A., Clayton, L. K., and Tenen, D. G. (1991) *Blood* **78,** 1826–1833
5. Simons, M., Wang, M., McBride, O. W., Kawamoto, S., Yamakawa, K., Gdula, D., Adelstein, R. S., and Weir, L. (1991) *Circ. Res.* **69,** 530–539
6. Leal, A., Endele, S., Stengel, C., Huehne, K., Loetterle, J., Barrantes, R., Winterpacht, A., and Rautenstrauss, B. (2003) *Gene* (*Amst.*) **312,** 165–171
7. Golomb, E., Ma, X., Jana, S. S., Preston, Y. A., Kawamoto, S., Shoham, N. G., Goldin, E., Conti, M. A., Sellers, J. R., and Adelstein, R. S. (2004) *J. Biol. Chem.* **279,** 2800–2808
8. Conti, M. A., Even-Ram, S., Liu, C., Yamada, K. M., and Adelstein, R. S. (2004) *J. Biol. Chem.* **279,** 41263–41266
9. Takahashi, M., Kawamoto, S., and Adelstein, R. S. (1992) *J. Biol. Chem.* **267,** 17864–17871
10. Kelley, C. A., Takahashi, M., Yu, J. H., and Adelstein, R. S. (1993) *J. Biol. Chem.* **268,** 12848–12854
11. Heath, K. E., Campos-Barros, A., Toren, A., Rozenfeld-Granot, G., Carlsson, L. E., Savige, J., Denison, J. C., Gregory, M. C., White, J. G., Barker, D. F., Greinacher, A., Epstein, C. J., Glucksman, M. J., and Martignetti, J. A. (2001) *Am. J. Hum. Genet.* **69,** 1033–1045
12. Franke, J. D., Dong, F., Rickoll, W. L., Kelley, M. J., and Kiehart, D. P. (2005) *Blood* **105,** 161–169
13. Hu, A., Wang, F., and Sellers, J. R. (2002) *J. Biol. Chem.* **277,** 46512–46517
14. Donaudy, F., Snoeckx, R., Pfister, M., Zenner, H. P., Blin, N., Di, S. M., Ferrara, A., Lanzara, C., Ficarella, R., Declau, F., Pusch, C. M., Nurnberg, P., Melchionda, S., Zelante, L., Ballana, E., Estivill, X., Van, C. G., Gasparini, P., and Savoia, A. (2004) *Am. J. Hum. Genet.* **74,** 770–776
15. Ma, X., Kawamoto, S., Hara, Y., and Adelstein, R. S. (2004) *Mol. Biol. Cell* **15,** 2568–2579
16. Takeda, K., Kishi, H., Ma, X., Yu, Z. X., and Adelstein, R. S. (2003) *Circ. Res.* **93,** 330–337
17. Pato, M. D., Sellers, J. R., Preston, Y. A., Harvey, E. V., and Adelstein, R. S. (1996) *J. Biol. Chem.* **271,** 2689–2695
18. Wang, F., Harvey, E. V., Conti, M. A., Wei, D., and Sellers, J. R. (2000) *Biochemistry* **39,** 5555–5560
19. Wang, F., Kovacs, M., Hu, A., Limouze, J., Harvey, E. V., and Sellers, J. R. (2003) *J. Biol. Chem.* **278,** 27439–27448
20. Cooper, J. A., Walker, S. B., and Pollard, T. D. (1983) *J. Muscle Res. Cell Motil.* **4,** 253–262
21. Facemyer, K. C., and Cremo, C. R. (1992) *Bioconjugate Chem.* **3,** 408–413
22. Kovacs, M., Wang, F., Hu, A., Zhang, Y., and Sellers, J. R. (2003) *J. Biol. Chem.* **278,** 38132–38140
23. Rosenfeld, S. S., Xing, J., Chen, L. Q., and Sweeney, H. L. (2003) *J. Biol. Chem.* **278,** 27449–27455
24. Maupin, P., Phillips, C. L., Adelstein, R. S., and Pollard, T. D. (1994) *J. Cell Sci.* **107,** 3077–3090
25. Kelley, C. A., Sellers, J. R., Gard, D. L., Bui, D., Adelstein, R. S., and Baines, I. C. (1996) *J. Cell Biol.* **134,** 675–687
26. Kolega, J. (2003) *Mol. Biol. Cell* **14,** 4745–4757
27. Lo, C. M., Buxton, D. B., Chua, G. C., Dembo, M., Adelstein, R. S., and Wang, Y. L. (2004) *Mol. Biol. Cell* **15,** 982–989
28. Meshel, A. S., Wei, Q., Adelstein, R. S., and Sheetz, M. P. (2005) *Nat. Cell Biol.* **7,** 157–164
29. Wylie, S. R., and Chantler, P. D. (2001) *Nat. Cell Biol.* **3,** 88–92
30. Tullio, A. N., Bridgman, P. C., Tresser, N. J., Chan, C. C., Conti, M. A., Adelstein, R. S., and Hara, Y. (2001) *J. Comp. Neurol.* **433,** 62–74
31. Spudich, J. A. (1994) *Nature* **372,** 515–518
32. Fisher, A. J., Smith, C. A., Thoden, J. B., Smith, R., Sutoh, K., Holden, H. M., and Rayment, I. (1995) *Biochemistry* **34,** 8960–8972
33. Geeves, M. A., and Holmes, K. C. (1999) *Annu. Rev. Biochem.* **68,** 687–728
34. Shih, W. M., and Spudich, J. A. (2001) *J. Biol. Chem.* **276,** 19491–19494
35. Houdusse, A., Szent-Gyorgyi, A. G., and Cohen, C. (2000) *Proc. Natl. Acad. Sci. U. S. A.* **97,** 11238–11243
36. Kliche, W., Fujita-Becker, S., Kollmar, M., Manstein, D. J., and Kull, F. J. (2001) *EMBO J.* **20,** 40–46
37. Kovacs, M., Toth, J., Nyitray, L., and Sellers, J. R. (2004) *Biochemistry* **43,** 4219–4226